Journal of Nuclear Materials 385 (2009) 601–605

Contents lists available at ScienceDirect

Journal of Nuclear Materials

journal homepage: www.elsevier.com/locate/jnucmat

Localization by TEM and EELS of deuterium trapping sites in CFC exposed to plasma irradiation in Tore Supra

N. Bernier [a,b,*], C. Brosset [a], F. Bocquet [b], E. Tsitrone [a], W. Saikaly [c], H. Khodja [d], V.Kh. Alimov [e], J.P. Gunn [a]

[a] Association EURATOM-CEA, CEA Cadarache, CEA/DSM/DRFC, 13108 Saint Paul Lez, Durance, France
[b] Institut IM2NP, UMR 6242, Université Paul Cézanne-Aix Marseille III, 13397 Marseille cedex 20, France
[c] CP2M, Université Paul Cézanne-Aix Marseille III, 13397 Marseille cedex 20, France
[d] Laboratoire Pierre Süe, CEA-CNRS UMR 9956, CEA Saclay, 91191 Gif-sur-Yvette, France
[e] Institute of Physical Chemistry and Electrochemistry, Russian Academy of Sciences, Leninsky prospect 31, 119991 Moscow, Russia

ARTICLE INFO

Article history:
Received 16 September 2008
Accepted 13 January 2009

ABSTRACT

Carbon fiber composite (CFC) Sepcarb® N11 is used in the tokamak Tore Supra as plasma-facing components. To investigate the fuel retention capability of this material, a mobile sample holder was used to expose CFC N11 samples to direct irradiation by the scrape-off layer plasma of Tore Supra at fluences up to 1×10^{25} m^{-2}. Deuterium (D) elemental mapping using nuclear reaction analysis for the most-exposed CFC sample showed that D retention occurs at depths greater than 8 μm due to the presence of deep (>3.5 μm) local retention sites. In this work, combining transmission electron microscopy (TEM) and electron energy-loss spectroscopy (EELS), we describe at a high spatial resolution where and how D atoms are trapped in these sites. TEM experiments performed on thin cross-sections of the plasma-modified surface show evidence of the presence of a 3.5 μm-thick deuterated amorphous carbon layer deposited on the CFC surface. We show that specific localized retention sites correspond to the filling of relatively large (~3 μm.) and deep (at least 3 μm below the initial CFC surface) cracks between fibres and matrix by the deuterated amorphous carbon layer.

1. Introduction

In modern thermonuclear fusion reactors, carbon fibre composites (CFC) are widely used as plasma-facing components, due to the low atomic number of carbon and the high-quality thermo-mechanical properties of CFC materials. However, interactions between CFC and hydrogen isotopes from the plasma lead to fuel retention in the vessel [1]. This raises crucial economic and safety issues for future fusion devices like ITER [2]. In the tokamak Tore Supra (TS), containing actively cooled CFC plasma-facing components, the deuterium (D) retention in the vessel during long pulses appears to be closely linked to the D implantation and migration into CFC materials [3,4]. The accurate characterization of this trapping mechanism is therefore crucial to maintain the use of CFC materials as plasma-facing components.

Dedicated experiments for this purpose were performed in TS via the controlled irradiation of CFC samples. After the first experiments during autumn 2003 [5], a second series of experiments was recently carried out in TS using a mobile sample holder to expose 10 CFC N11 samples to direct irradiation by the scrape-off layer up to deuterium fluences of 10^{25} m^{-2}. Nuclear reaction analysis (NRA), using D(^{3}He,p)^{4}He reactions [6], was performed to determine the D depth profile in plasma-exposed CFC samples as a function of discharge conditions. Fig. 1 illustrates the NRA-measured D profile up to a depth of 8 μm for the most irradiated CFC sample, B1. This profile exhibits two characteristic zones: a constant D concentration around 35 at.% from the surface down to a depth of about 3.7 μm, followed by a tail extending beyond 8 μm. Previously, a similar D depth profile with a tail extending beyond 14 μm was found for the CFC N11 and NB31 irradiated by 30–200 eV D ions both from ion beams and plasma devices in laboratory [7]. However, in dense pyrolytic graphite, the implantation range is limited by the ion incident energy (typically around 10 nm for 200 eV D ions) [8]. Therefore, experiments carried out in TS highlight the characteristic behaviour of CFC during plasma irradiation, and also raise issues related to fuel retention deep into the plasma-facing components (for instance choice of tritium removal techniques [9]).

Given the known structural heterogeneity of CFC materials (i.e., fibres of diameter 6–7 μm embedded in a matrix), it is crucial to ensure that the spatially averaged (over about 3 mm^2) D depth profile shown in Fig. 1 is representative of the D retention in CFC on a micrometer scale. Spatially resolved NRA [10] was thus performed to determine the lateral distribution of D retention. In this technique, a 3 MeV ^{3}He ion beam (2×2 μm^2) is used to produce

* Corresponding author. Address: Association EURATOM-CEA, CEA Cadarache, CEA/DSM/DRFC, 13108 Saint Paul Lez, Durance, France. Tel.: +33 (0) 438 784 870; fax: +33 (0) 438 785 273.
E-mail address: n.bernier@univ-cezanne.fr (N. Bernier).

0022-3115/$ - see front matter Crown Copyright © 2009 Published by Elsevier B.V. All rights reserved.
doi:10.1016/j.jnucmat.2009.01.031

D(^{3}He, p)^{4}He reactions. Three-dimensional D elemental mapping is achieved by electrostatic beam scanning. Results [10] showed that from the surface down to a depth of 3.7 μm, corresponding to the D plateau displayed in Fig. 1, the D concentration is homogeneously distributed. On the contrary, the D retention is heterogeneous at higher depths as can be seen from Fig. 2 which shows the distribution of D retention at a depth of 5 μm. This spatially resolved NRA image, representative of the D distribution at depths higher than 3.7 μm, reveals that D is trapped in localized sites deep into plasma-exposed CFC materials. In order to structurally characterize these D-rich zones, tracking by scanning electron microscopy (SEM) was used in spatially resolved NRA experiments. It is shown [10] that D-rich zones are always located in the vicinity of fibres oriented perpendicular to the CFC surface. For instance, the SEM image shown in Fig. 3 corresponds to the D-rich region indicated by the square in Fig. 2.

The aim of this work is to propose a clear understanding for the deep retention of D in plasma-exposed CFC materials. However, to determine where and how D atoms are trapped in the D-rich regions revealed by the NRA–SEM combination, three conditions are required: (i) a higher spatial resolution, (ii) a cross-section to visualize the structure as a function of the depth, (iii) chemical analysis to detect the presence of chemisorbed D atoms. The technique of choice fulfilling these criteria is transmission electron microscopy (TEM). The local coupling of structural information provided by TEM with chemical information is performed using electron energy-loss spectroscopy (EELS). Indeed, this technique allows for a spatial resolution of 10 nm^2 the characterization of carbon atom hybridization state, which is particularly affected by the amount of D chemisorbed.

In Section 2, experimental details are given. In Section 3, we show, using the TEM–EELS combination, how D atoms are trapped in the different zones of plasma-exposed CFC with a particular focus on those located deep into the material. After a short summary, a mechanism explaining the deep retention of D is proposed in Section 4.

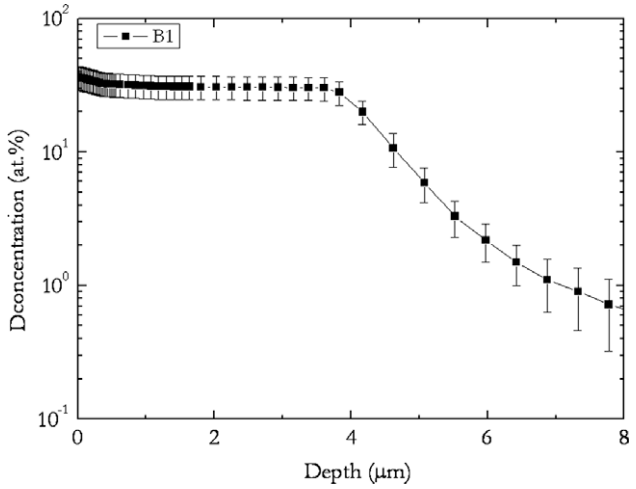

Fig. 1. Deuterium depth profile for the most-exposed CFC N11 sample, named B1, obtained by D(^{3}He,p)^{4}He nuclear reaction [6].

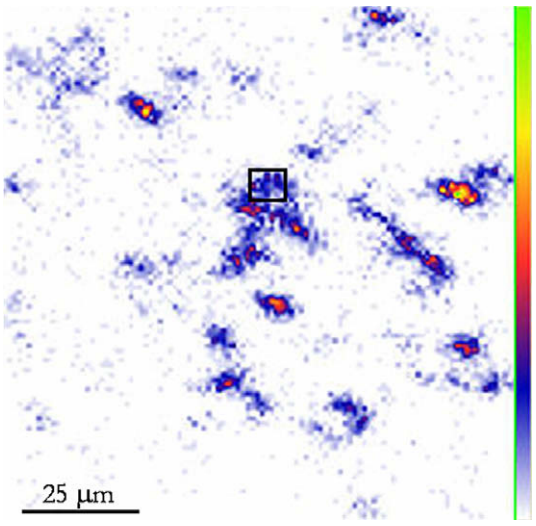

Fig. 2. Deuterium mappings from the B1 sample obtained by scanning a ^{3}He microbeam and filtering the NRA spectrum with region of interest covering depths ranging from 4 to 6 μm. The D concentration follows a code of colours (the lowest and the highest D concentration, respectively, correspond to white and green) [10]. The region confined in squares corresponds to Fig. 3 (For interpretation of the references to colour in this figure legend, the reader is referred to the web version of this article.).

2. Experimental

2.1. Sample exposure

A sample holder equipped with Langmuir probes and thermocouples has been installed on the fast-scanning probe system in TS. It exposed 10 CFC samples to plasma irradiation in the scrape-off layer. The cumulative ion fluence, the mean ion incident energy, and the thermal history are simultaneously measured to determine the plasma-CFC interactions as a function of discharge conditions. We study here the most irradiated sample named B1 (deuterium fluence 10^{25} m^{-2}, mean D energy 500 eV, mean sample temperature 700 K). Note that mean D energy and mean sample temperature are rough estimates given the strong variations during the campaign (see Ref. [5] for more details).

The CFC sample is the Sepcarb® N11 type manufactured by SEP (Bordeaux, France): the composite was fabricated from three-dimensional PAN-based carbon fibres, the matrix being formed by carbon vapour infiltration and graphitized afterwards at elevated temperatures. The fibre volume fraction is of 30%, and the density is equal to 1.8 g cm^{-3}. The CFC samples were mechanically cut from CFC blocks and no additional treatment was carried out. CFC zones studied by NRA were chosen such that fibres are oriented perpendicular to the surface corresponding to the highest thermal conductivity.

2.2. Sample preparation

The thin foils for TEM analysis were prepared by focused ion beam (FIB) milling (FIB 200TEM FEI machine using a 30 kV Ga^+ ion beam) [11]. This technique allows for the extraction of site-specific cross-sections having near parallel sides over a dozen or so micrometers. Nevertheless, the use of high-energy ions for milling may create amorphous damage layers in crystalline materials. To minimize this damage, an optimized FIB procedure was developed in our laboratory [12], which partly consists of a final low voltage (10 kV) and low current (50 pA) ion beam to minimize the damaged layer on each side of the FIB lamellae as well as a final cut normal to the surface to avoid sidewall-ion implantation. A FIB procedure relatively similar to our optimized one turned out to be effective when applied to CFC materials with a graphitic matrix [13].

2.3. TEM and EELS analysis

The experiments discussed here were performed on a Jeol 2010F TEM operating at 200 kV, equipped with a Gatan Imaging

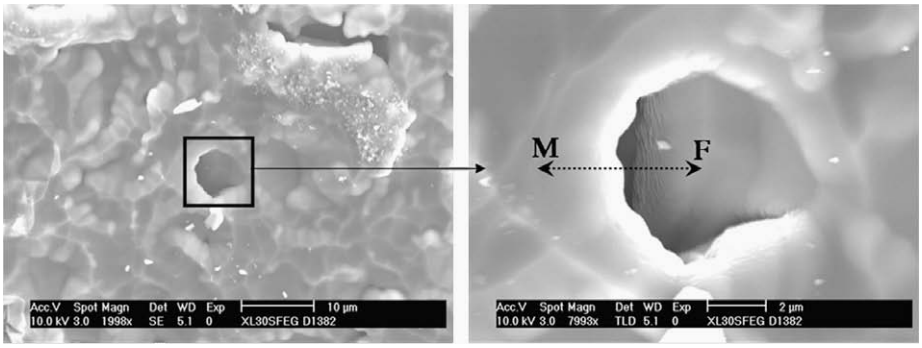

Fig. 3. SEM image corresponding to the deuterium-rich zone indicated by the square in Fig. 2. The dotted arrow corresponds to the zone where the FIB lamella shown in Fig. 6 is extracted. M and F, respectively, correspond to the matrix and fibre zone.

Filter (GIF 200). EELS spectra at the K edge of carbon, or C–K edge EELS spectra, were acquired for all specimen in diffraction mode with a channel dispersion of 0.3 eV. The spectral energy resolution was evaluated at about 1 eV. The typical acquisition times for the C–K edge and for the low-loss (i.e., energy losses smaller than about 100 eV) were, respectively, 15 s and 0.1 s, these two spectral portions being acquired with the same geometrical configuration. Spectra were acquired with an incident convergence semi-angle and a collection semi-angle both equal to about 2.1 mrad. As commonly performed, the initial spectral treatment mainly consists of two steps [14]: a background subtraction performed by the pre-edge window technique and a multiple scattering removal performed by a standard Fourier-ratio deconvolution procedure. In addition, all spectra were acquired on thin sample areas, in order to ensure a correct spectral treatment [14].

We acquired EELS spectra to quantitatively extract the fraction of sp^2-bonded carbon atoms. The quantification is based on the extraction of the 1s to $\pi*$ peak located at about 285 eV in the C–K edge EELS spectrum. This peak is indeed exclusively provided by carbon atoms in hybridization sp^2, such that the comparison of the $\pi*$ peak intensity in the unknown material with that in a suitable known standard is a direct measure of the sp^2 fraction [15]. Since graphite exhibits a perfectly known crystallographic structure (composed only of sp^2 hybrid atoms) and does not suffer from rapid irradiation damage under electron beam, this material is used in this work as a standard to determine sp^2 fractions. We showed in previous studies how to avoid issues related to preferential orientation effects in graphite EELS spectra [16] and how to proceed the extraction of the 1s to $\pi*$ peak in the C–K edge EELS spectra [17].

3. Results and discussion

The TEM-EELS study of the plasma-exposed CFC is performed in two steps. The first one consists in analysing representative zones of the largest part of the plasma-exposed CFC surface in order to obtain general features of D retention in CFC. The second one consists in performing FIB lamellae in D-rich zones revealed by spatially resolved NRA in order to determine how D atoms are trapped deep into the material.

Fig. 4 shows a TEM image of a FIB lamella extracted from a representative zone of the largest part of the plasma-exposed CFC surface. This figure presents a cross-section revealing the CFC microstructure from the surface down to about 7 μm deep (FIB depth-limit). Two characteristic zones can be distinguished: an amorphous layer with a thickness of about 3.5 μm (as evidenced by the halo in the power spectrum displayed in the inset of Fig. 4), and an underlying zone exhibiting the same graphitic structure (as revealed by the spots in the second inset) as in CFC before plasma irradiation. We also checked that the pores localized in the CFC matrix (i.e., white zones in Fig. 4) are already present in the virgin CFC, and are thus not caused by plasma irradiation.

From the FIB lamella image given in Fig. 4, we can conclude that the D plateau from the surface up to about 3.7 μm deep observed in the D depth profile in Fig. 1 corresponds to the D atoms trapped in the amorphous layer. A C–K edge EELS spectrum of this deposited amorphous layer is shown in Fig. 5 (spectrum a). Two features of this spectrum have to be mentioned: (i) the 1s to $\sigma*$ peak is centred at about 295 eV while this peak in graphite is centred at a lower energy (spectrum b), (ii) unlike in graphite EELS spectra, there is no fine structure after the 1s to $\sigma*$ peak in the spectrum displayed in spectrum a. Therefore, the EELS spectrum acquired in the deposited amorphous layer is typical of amorphous carbon EELS spectra [18]. In addition, the amorphous layer EELS spectrum, following the quantification process [17], corresponds to a sp^2 fraction of 72%. Combining this value with the D concentration of 35 at.% obtained by NRA, and using the ternary phase diagram in amorphous carbon – hydrogen alloys given in Ref. [19], we can show that the electronic structure of the deposited amorphous layer in the plasma-exposed CFC is consistent with published data referring to amorphous hydrogenated carbon layers produced in laboratory by plasma enhanced chemical vapour deposition [19]. It can be reasonably thought that the growth mechanism of the deposited amorphous layer is due to either sticking of C_xD_y molecules or impact on the CFC surface of carbon atoms (coming from different parts of TS) simultaneously bombarded by a D flux from plasma.

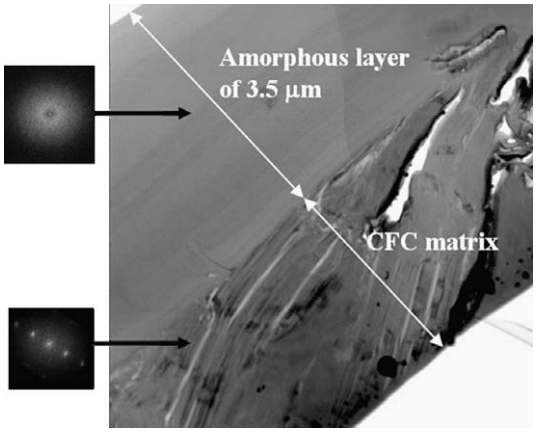

Fig. 4. TEM image revealing the B1 sample microstructure from the surface up to about 7 μm deep. We note the presence of a 3.5 μm-thick amorphous carbon layer deposited onto the initial CFC matrix surface. The insets show diffraction pattern in the amorphous layer and graphitic matrix.

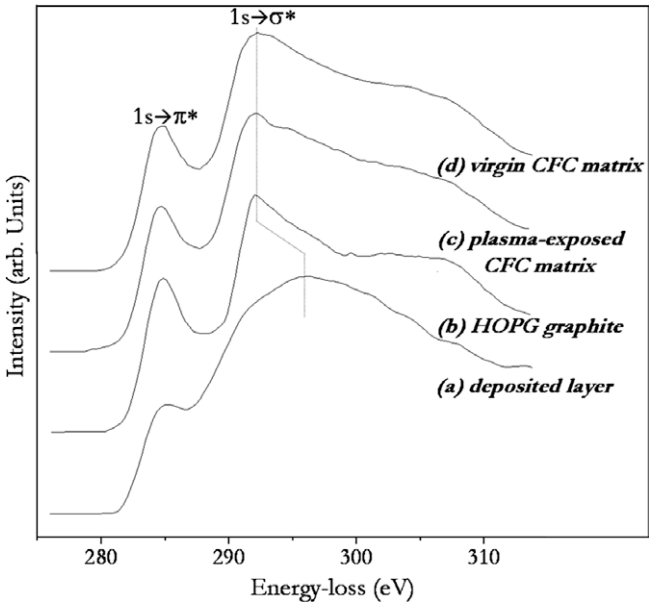

Fig. 5. EELS spectra acquired (a) in the deposited amorphous layer of B1, (b) on highly order pyrolytic graphite (HOPG) with the graphene sheets parallel to the optical microscope axis (c) 20 nm below the interface between the amorphous layer and the matrix, (d) in the matrix of a non-irradiated CFC sample. Note that in spectrum (a), the $1s \rightarrow \sigma^*$ peak is shifted approximately 3.8 eV to higher energies.

We verified on five FIB lamellae extracted from different CFC zones that results showed the same trends: the EELS spectra displayed in Fig. 5 are thus representatives of these zones. Spectrum c shows a typical EELS spectrum (sp^2 fraction of 96 ± 4%) acquired in a zone located 20 nm under the deposited amorphous layer. The TEM images of this zone (not shown here) evidence a graphitized structure with (002) spots in diffraction patterns corresponding to the resolved lattice of perfect graphite (i.e., a spacing of 0.33 nm related to (002) planes). Given both the sp^2 fraction value and the graphitized structure, we can conclude a total absence of chemisorbed D atoms in the matrix as soon as the interface amorphous layer – matrix is reached. It also has to be noticed that the EELS spectrum of the virgin CFC matrix given in Fig. 5(d) is strictly identical to that of the plasma-exposed CFC matrix, and thus lead to the same sp^2 fraction of 96%. The comparison of sp^2 fractions before and after plasma irradiation is another relevant approach to conclude that matrix exhibits no sign of D retention. We used this later mentioned approach in the case of fibres constituting 30 vol.% of CFC N11: as we showed that fibres EELS spectra are identical before and after plasma irradiation, we conclude a negligible retention in plasma-exposed CFC fibres. From these results, the D trapping sites deep into the plasma-exposed CFC, evidenced by the spatially resolved NRA D mapping shown in Fig. 2, are not located in fibres and matrix.

In order to precisely characterize these deeply located D trapping sites, FIB lamellae were extracted from D-rich zones revealed by the NRA–SEM combination. For instance, Fig. 6 shows a TEM image of the FIB lamella (positioned on a supporting carbon film) extracted from the zone represented by the dotted arrow in Fig. 3. It has to be noticed that the TEM–EELS study showed once more no sign of D retention in the matrix and the fibres. Fig. 6 reveals the presence of a crack about 3–4 μm large between the fibre (labelled F) and matrix (labelled M). Although the probed depth is limited by the FIB technique, these cracks are believed to extend to depths at least 3 μm under the initial CFC surface. From the different FIB lamellae, we can also note that fibres in the direct vicinity of cracks regularly present an irregular shape located some microns below the mean surface of the CFC matrix. This behaviour is thought to

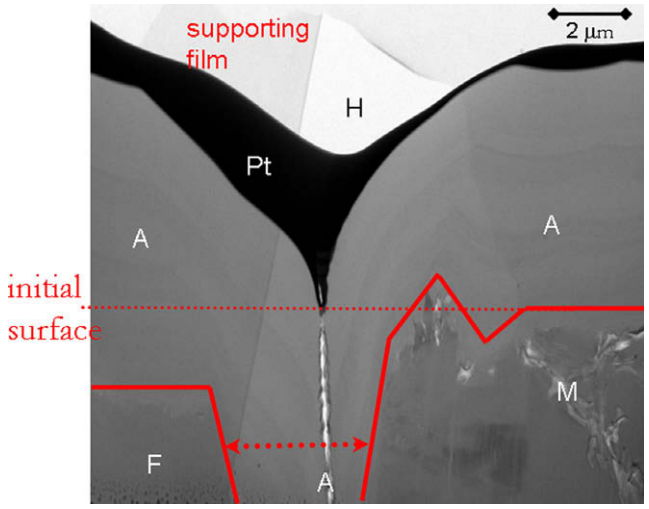

Fig. 6. TEM image of the FIB lamella extracted from the zone represented by the dotted arrow in Fig. 3. We note that the amorphous layer (A) penetrates and fills the large (~3 μm large), deep crack between the fibre (F) and the matrix (M). Contrast variation in the layer A is only due to the presence of the hole (H) in the supporting carbon film allowing the acquisition of EELS spectra without contribution of the supporting film.

be issued from the fibre breaking during the mechanical cut of CFC blocks. The black layer (labelled Pt), corresponding to the protective Pt layer deposited before the FIB etching procedure, follows the same contours as an underlying grey layer labelled A (for amorphous). This layer, from the top to the bottom of the FIB lamellae, is homogeneous (note that the contrast variation in the layer is only due to the presence of the hole in the carbon supporting film, labelled H, allowing to acquire EELS spectra without contribution of the supporting film) and exhibits the same sp^2 fraction of 72% as the layer shown in Fig. 4. Therefore, it can be reasonably thought that the amorphous layer present in the cracks is exactly the same as that deposited on the initial CFC surface.

From all these results, the presence of deeply located D-rich zones revealed by spatially resolved NRA can be interpreted in the following manner: a deuterated amorphous carbon layer is deposited onto the CFC surface and exactly follows the local micrometric topography. This results in the filling of large gaps between

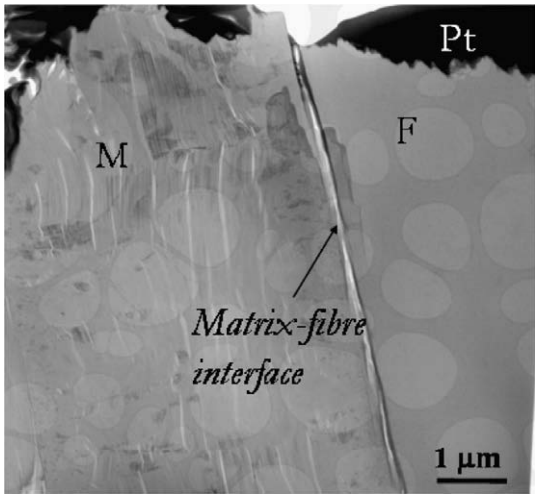

Fig. 7. TEM image illustrating the presence of intrinsic narrow (~50 nm large) crack between fibres and matrix in the CFC N11. The circular contrast variation is only due to the presence of holes in the supporting film.

matrix and fibres yielding D retention deep into the material. The lateral heterogeneity of this retention has two explanations:

(i) The absence of emerging fibres in some CFC zones.
(ii) When samples are mechanically cut from CFC blocks, only some fibres smash below the mean CFC surface and lead to large cracks.

Indeed, Fig. 7 clearly shows a fibre exhibiting a plane surface at the same height as the CFC matrix surface. In this case, in place of large cracks between the fibres and the matrix, we note the presence of an intrinsic nanometer crack which could offer a way for D atoms to migrate deeper into the material. Analysis of these intrinsic cracks after plasma exposition is under progress.

4. Conclusion

In order to investigate the D retention capability of CFC materials and to explain the particle balance results in Tore Supra during long discharges, irradiation of CFC N11 samples at fluence up to $1 \times 10^{25}\ m^{-2}$ has been achieved in TS. NRA and SEM analysis of the most-exposed CFC sample, named B1, previously revealed the presence of deep D-rich sites located in the vicinity of fibres. These sites account for the long profile tail extending beyond 8 μm in the D depth profile of the B1 sample. For a precise characterization of these sites and for a detailed understanding of D retention mechanisms, structural and chemical information on a submicron scale are required. Therefore, in this work we have carried out a combined TEM–EELS study of the B1 sample.

Results can be summarized in three main points:

(i) The investigation of the CFC microstructure before and after plasma irradiation gives evidence of the growth of a 3.5 μm-thick deuterated carbon layer on the CFC surface. This layer can be unambiguously related to the D plateau observed in the D depth profile measured by NRA.
(ii) TEM and EELS analysis demonstrated that there is no sign of D retention in matrix and fibres.
(iii) D trapping sites located deep into the plasma-exposed CFC correspond to the filling of large (3–4 μm) and deep (at least 3 μm below the initial CFC surface) cracks between fibres and matrix by the deposited carbon layer. These cracks likely appear when fibres smash during the mechanical cut process of CFC blocks.

We can conclude that the deep and heterogeneous D retention reported earlier is mainly due to the deposition of a deuterated amorphous carbon layer which penetrates and fills the large, deep cracks between some fibres and matrix. The question then arises as to whether D is migrating in combination with carbon, for instance via hydrocarbon radicals. Experiments investigating high-fluence D implantation mechanisms in CFC materials without simultaneous C fluxes would certainly provide valuable information regarding this question. We can also wonder whether the same mechanism of D infiltration is relevant for the nanometer cracks intrinsically present in the CFC materials. This point is of major importance because these cracks, though narrower, would potentially allow D atoms to migrate deeper in the material. These cracks could therefore offer a direct, simple path for D atoms to penetrate different kinds of pores in the material.

References

[1] G. Federici, C.H. Skinner, J.N. Brooks, J.P. Goad, C. Grisolia, A.A. Haasz, et al., Nucl. Fus. 41 (2001) 1967.
[2] J. Roth, E. Tsitrone, A. Loarte, Nucl. Instrum. and Meth. B 258 (2007) 253.
[3] E. Tsitrone, J. Nucl. Mater. 363–365 (2007) 12.
[4] J. Bucalossi, C. Brosset, B. Pégourié, E. Tsitrone, E. Dufour, A. Eckedahl, et al., J. Nucl. Mater. 363–365 (2007) 12.
[5] J.P. Gunn, L. Begrambekov, C. Brosset, A. Gordeev, T. Loarer, E. Miljavina, et al., J. Nucl. Mater. 337–339 (2005) 644.
[6] V.Kh. Alimov, D.A. Komarov, J. Roth, M. Mayer, S. Lindig, J. Nucl. Mater. 349 (2006) 282.
[7] J. Roth, V.Kh. Alimov, A.V. Golubeva, R.P. Doerner, J. Hanna, E. Tsitrone, et al., J. Nucl. Mater. 363–365 (2007) 822.
[8] B.L. Doyle, W.R. Wampler, D.K. Brice, S.T. Picraux, J. Nucl. Mater. 93&94 (1980) 551.
[9] R.A. Causey, J.N. Brooks, G. Federici, Fus. Eng. Des. 61&62 (2002) 525.
[10] H. Khodja, C. Brosset, N. Bernier, Nucl. Instrum. and Meth. B 266 (2008) 1425.
[11] M.H.F. Overwijk, F.C. Van den Heuvel, C.W.T. Bulle-Lieuwma, J. Vac. Sci. Technol. B11 (1993) 2021.
[12] L. Alexandre, K. Rousseau, C. Alfonso, W. Saikaly, L. Fares, C. Grosjean, A. Chara, Micron 39 (2008) 294.
[13] H. Mucha, T. Kato, S. Arai, H. Saka, K. Kuroda, B. Wielage, J. Electron Microsc. 54 (2005) 43.
[14] R.F. Egerton, Electron Energy Loss Spectroscopy in the Electron Microscope, Plenum, New York, London, 1996.
[15] S.D. Berger, D.R. McKenzie, P.J. Martin, Philos. Mag. Lett. 57 (1988) 285.
[16] F. Bocquet, N. Bernier, W. Saikaly, C. Brosset, J. Thibault, A. Chara, Ultramicroscopy 107 (2007) 81.
[17] N. Bernier, F. Bocquet, A. Allouche, W. Saikaly, C. Brosset, J. Thibault, A. Charai, J. Electron Spectrosc. Relat. Phenom. 164 (2008) 34.
[18] J. Yuan, L.M. Brown, Micron 31 (2000) 515.
[19] J. Robertson, Mater. Sci. Eng. 37 (2002) 129.